Acta Crystallographica Section A
Foundations of Crystallography
ISSN 0108-7673

Received 24 December 2001
Accepted 24 June 2002

Rocking-curve width of sagittally bent Laue crystals

Z. Zhong,* C. C. Kao, D. P. Siddons and J. B. Hastings†

National Synchrotron Light Source, Brookhaven National Laboratory, Upton, NY 11973, USA. Correspondence e-mail: zhong@bnl.gov

The use of bent asymmetric Laue crystals to sagittally focus high-energy synchrotron X-rays calls for an understanding of the mechanisms affecting X-ray diffraction by such crystals. The rocking-curve width, a measurable quantity directly related to the distortion of the lattice planes, is the necessary first step towards such an understanding. A model is formulated for assessing the rocking-curve widths of sagittally bent Laue crystals, considering the elastic anisotropy. A method for depth-resolved measurement of the rocking curves was also developed to verify the model. The model successfully explains the wide range of rocking-curve widths of a large number of reflections from silicon crystals with two different orientations.

1. Introduction

We recently showed that sagittally bent asymmetric Laue crystals, diffracting in the vertical plane, can focus X-rays horizontally (Zhong *et al.*, 2001*a*,*b*). Their use is preferable to that of Bragg crystals at higher X-ray energies owing to the much reduced footprint of the beam. Moreover, Laue crystals allow us to take advantage of anticlastic bending to realize the inverse-Cauchois geometry in the meridional plane, resulting in better energy resolution than achievable with traditional sagittal focusing by Bragg crystals. Modes of implementing sagittally bent Laue crystals in single- and double-crystal horizontally focusing monochromators, suitable for high-energy synchrotron X-rays, were suggested and have been verified experimentally.

Experiments showed that, in addition to the gain in intensity due to focusing, sagittally bent Laue crystals increased the flux of the focused X-ray beam by about an order of magnitude over that of perfect crystals (Zhong *et al.*, 2001*b*). This effect is mainly due to a significant increase in the width of the rocking curve, a result of lattice distortion introduced by sagittal bending. The extent of this increase depended on the crystal's orientation and the asymmetry angle of the reflection used. Thus, it is important to understand quantitatively how sagittal bending leads to the broadening of the rocking curve, so that we can simulate diffraction properties, such as angular/energy acceptance and reflectivity, to aid in designing monochromators.

Meridionally bent crystals (crystals bent in the diffraction plane) have been used previously to meridionally focus X-rays and neutrons. A lamellar model has been used successfully in both the Bragg and Laue geometries to explain X-ray and neutron diffraction by such crystals (Egert & Dachs, 1970; Albertini *et al.*, 1976; Boeuf *et al.*, 1978; Mikula *et al.*, 1984). According to the model, the rocking-curve width of a Laue crystal, a measurable quantity, corresponds directly to the change in Bragg angle and rotation of lamellae across its depth. Theories have been derived for the angular acceptance of meridionally bent isotropic crystals (Caciuffo *et al.*, 1987; Popovici *et al.*, 1988; Erola *et al.*, 1990; Hiraoka *et al.*, 2001). Similar treatments were worked out for meridionally bent anisotropic crystals (Kalman & Weissmann, 1983; Schulze *et al.*, 1998). Although the isotropic model is adequate for most applications of meridionally bent crystals, elastic anisotropy was found to play a role in explaining the observed rocking-curve widths in some special cases (Hartlaub, 1996).

In meridionally bent crystals, the bending plane is the same as the plane of diffraction, and bending directly influences the change of lattice spacing and the tilting of lattice planes (Lienert *et al.*, 1998). On the other hand, sagittal bending affects the diffraction process occurring perpendicular to the plane of bending, but in a less direct way. Our earlier attempt to adapt a model for meridionally bent crystals to sagittally bent ones, by simply considering anticlastic bending (Zhong *et al.*, 2001*b*), was unsatisfactory. Sagittal bending typically is an order of magnitude more severe than meridional bending, and introduces significant extra modifications to the lattice spacing and tilting of the lamellae than are accounted for by anticlastic bending alone.

In this work, an analytical model for the rocking-curve width of X-ray diffraction by sagittally bent Laue crystals is derived from first principles, taking into consideration the elastic anisotropy of the crystals. The calculated angular-acceptance widths, including their signs, for ten different reflections on sagittally bent crystals of two representative orientations, were verified experimentally by a depth-resolved rocking-curve measurement specifically designed for this purpose.

† Present address: SSRL, 2575 Sand Hill Road, Menlo Park, CA 94025, USA.

2. Rocking-curve width

Fig. 1 depicts a sagittally bent crystal diffracting in the Laue mode to illustrate the crystal's orientation, the direction of bending, and the diffraction planes in the coordinate system. The planar crystal, depicted in the yz plane, is sagittally bent around the y axis; and the resulting anticlastic bending is around the z axis. The diffraction vector **H** lies in the diffraction plane which coincides with the xy plane.

The coupling between the bending in the sagittal plane and the lattice distortion in the diffraction plane is orientation dependent. Thus, it is necessary to take into consideration the anisotropy of the crystal. From results obtained for plates of constant cross section bent by equal but opposite moments, the displacement field is (Voigt, 1928; Kalman & Weissmann, 1983; Chukhovskii *et al.*, 1994)

$$\begin{aligned} u_x &= E[x^2 S_{13} - y^2 S_{23} - zyS_{43} - z^2 S_{33}] \\ u_y &= E[x^2 S_{63} + 2xyS_{23} + xzS_{43}] \\ u_z &= E[x^2 S_{53} + xyS_{43} + 2xzS_{33}], \end{aligned} \tag{1}$$

where S_{ij} are the elastic compliances of the crystal for a specific orientation, $u_{x,y,z}$ are displacements in the x, y and z directions, respectively, and E is a constant related to the bending moment and moment of inertia of the crystal. E is positive for bending as shown in Fig. 1.

Equation (1) assumes the crystal to be a free-standing one. However, actual crystals used for experiments are typically constrained by bending devices. The ratio between the meridional- and sagittal-bending radii then is modified by a factor C through $R_m = R_s/(CS'_{23})$, where $S'_{23} \equiv S_{23}/S_{33}$ is the Poisson ratio of the crystal, and C is a constant that accounts for the shape of, and the constraints on, the crystal (Krisch *et al.*, 1991; Quintana *et al.*, 1995; Suortti & Schulze, 1995; Yoneda *et al.*, 2001). Without elaborating on the details of the elastic deformation of the crystal under complex boundary conditions, the S_{23} in (1) is simply replaced by CS_{23} to account for these effects. Equation (1) then becomes

$$\begin{aligned} u_x &= E[x^2 S_{13} - y^2 CS_{23} - zyS_{43} - z^2 S_{33}] \\ u_y &= E[x^2 S_{63} + 2xyCS_{23} + xzS_{43}] \\ u_z &= E[x^2 S_{53} + xyS_{43} + 2xzS_{33}]. \end{aligned} \tag{2}$$

The sagittal bending radius is $R_s = -1/(2S_{33}E)$; R_s is negative for the situation shown in Fig. 1. In the diffraction plane, the anticlastic bending radius is $R_m = -1/(2CS_{23}E)$.

For diffraction occurring in the xy plane, the bent crystal is approximated by a stack of perfect lamellae with a gradually changing orientation and lattice spacing. The angle the crystal needs to rotate to obtain the Bragg condition for the lamellar at depth T is

$$\Delta\theta(T) = -\Delta\theta_{\rm rot}(T) + \Delta\theta_B(T), \tag{3}$$

where $\Delta\theta_{\rm rot}(T)$ is the change in the angle between the lattice planes and the incident X-rays, at depth T along the incident beam's path, with respect to the angle at the point where the beam enters the crystal ($T = 0$). $\Delta\theta_B(T)$ is the corresponding change in the Bragg angle. T is defined to increase along the beam's trajectory.

The change in the lattice orientation, $\Delta\theta_{\rm rot}(T)$, is calculated by following the rotation of a segment of the lattice plane, of small length l, in the diffraction plane. Inset A in Fig. 1 shows a small segment, (dx, dy, dz) before bending (solid vector) and afterwards (dashed vector). The displacement of the segment, (du_x, du_y, du_z), can be calculated by

$$du_{x,y,z} = \frac{\partial u_{x,y,z}}{\partial x}dx + \frac{\partial u_{x,y,z}}{\partial y}dy + \frac{\partial u_{x,y,z}}{\partial z}dz. \tag{4}$$

According to the coordinate system defined in Fig. 1, $dx = -l\cos\chi$, $dy = l\sin\chi$ and $dz = 0$, where χ is the asymmetry angle for the Laue reflection, defined as the angle between the lattice planes and the crystal's surface normal. For the present discussion, χ is positive if the diffraction vector **H** is in the first and third quadrants, as is the case for both the upper- and lower-case reflections shown in Fig. 1. χ is negative for diffraction vectors that are in the second and fourth quadrants.

The change in the angle between the lattice planes and the incident beam, $d\theta_{\rm rot}(x, y, 0)$, from the neutral angle before bending, at a position $(x, y, 0)$ in the crystal, is represented by the small angular change of the segment in the plane of diffraction,

$$d\theta_{\rm rot}(x, y, 0) = \pm(du_x \sin\chi + du_y \cos\chi)/l. \tag{5}$$

The upper sign is used when the diffraction vector is in the first and second quadrants ($\mathbf{H}\cdot\mathbf{y} > 0$), shown by the solid **H** vector in Fig. 1. The lower sign is used when **H** is in the third and fourth quadrants ($\mathbf{H}\cdot\mathbf{y} < 0$), represented by the dashed **H**. du_z does not affect $\theta_{\rm rot}$ because only displacement in the diffraction plane causes lattice rotation in this plane.

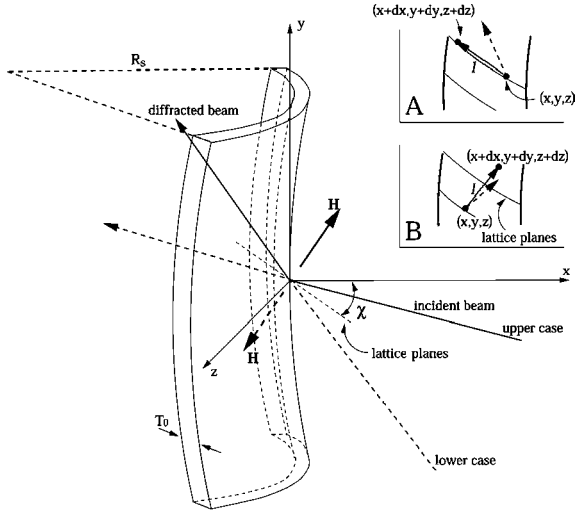

Figure 1
A sagittally bent crystal, diffracting in the the Laue mode. Inset *A* shows the mechanism for lattice rotation. Inset *B* shows the mechanism for *d*-spacing change.

Using (2), (4) and (5), we have

$$\mathrm{d}\theta_{\rm rot}(x, y, 0) = \pm (1/R_s)[x(S'_{13} - CS'_{23}) \sin\chi\cos\chi + yCS'_{23} + (z/2)S'_{43} + xS'_{63}\cos^2\chi], \quad (6)$$

where $S'_{ij} \equiv S_{ij}/S_{33}$.

We note that the bent crystal's angular acceptance is not affected by the absolute lattice rotation itself but by the relative change of this rotation along the beam's path. If we assume that the incident X-rays meet the crystal's surface at (0, 0, 0), then a point $(x, y, 0)$ along the path is related to its depth, T, in the crystal by

$$\begin{aligned} x &= -T \\ y &= T\tan(\chi \mp \theta_B), \end{aligned} \quad (7)$$

where θ_B is the Bragg angle for the reflection. Along the incident beam's path, the change in lattice rotation, $\Delta\theta_{\rm rot}(T)$, at depth T in the crystal, relative to that at $T = 0$, is calculated using (6) and (7),

$$\begin{aligned} \Delta\theta_{\rm rot}(T) &= \mathrm{d}\theta_{\rm rot}(x, y, 0) - \mathrm{d}\theta_{\rm rot}(0, 0, 0) \\ &= \mp (T/R_s)[(S'_{13} - CS'_{23})\sin\chi\cos\chi \\ &\quad - CS'_{23}\tan(\chi \mp \theta_B) + S'_{63}\cos^2\chi]. \end{aligned} \quad (8)$$

The $\Delta\theta_B(T)$ term in (3) is caused by the difference in expansion or compression of the lattice's d spacing at different depths. Inset B in Fig. 1 shows a small segment $(\mathrm{d}x, \mathrm{d}y, \mathrm{d}z)$, aligned parallel to the diffraction vector, before bending (solid vector) and afterwards (dashed vector). According to the figure, $\mathrm{d}x = l\sin\chi$, $\mathrm{d}y = l\cos\chi$ and $\mathrm{d}z = 0$.

The length change in the segment, $\mathrm{d}l$, resulting from bending, is

$$\mathrm{d}l(x, y, 0) = \mathrm{d}u_x \sin\chi + \mathrm{d}u_y \cos\chi, \quad (9)$$

where $\mathrm{d}u_{x,y}$ can be calculated using (4).

The change of Bragg angle at $(x, y, 0)$, owing to the change in lattice spacing at that position, then is calculated using (4) and (9),

$$\begin{aligned} \mathrm{d}\theta_B(x, y, 0) &= -[\mathrm{d}l(x, y, 0)/l]\tan\theta_B \\ &= (1/R_s)x\tan\theta_B[S_{13}\sin^2\chi + S_{63}\sin\chi\cos\chi \\ &\quad + CS_{23}\cos^2\chi]. \end{aligned} \quad (10)$$

Equations (10) and (7) give the relative change in Bragg angle, $\Delta\theta_B(T)$, along the beam's trajectory,

$$\begin{aligned} \Delta\theta_B(T) &= \mathrm{d}\theta_B(x, y, 0) - \mathrm{d}\theta_B(0, 0, 0) \\ &= -(T/R_s)\tan\theta_B[S'_{13}\sin^2\chi + CS'_{23}\cos^2\chi \\ &\quad + S'_{63}\sin\chi\cos\chi]. \end{aligned} \quad (11)$$

As expected, $\Delta l/l$, an intrinsic property of the crystal, does not depend on the reflection used. The resulting change in Bragg angle thus is the same for both the upper and lower cases, and is only related to the Bragg angle through the term $\tan\theta_B$. From (3), (8), and (11), the angle the crystal needs to rotate to find the Bragg condition for a lamella at depth T is

$$\begin{aligned} \Delta\theta(T) &= (T/R_s)\{\pm[(S'_{13} - CS'_{23})\sin\chi\cos\chi - CS'_{23}\tan(\chi \mp \theta_B) \\ &\quad + S'_{63}\cos^2\chi] - \tan\theta_B[S'_{13}\sin^2\chi + CS'_{23}\cos^2\chi \\ &\quad + S'_{63}\sin\chi\cos\chi]\}. \end{aligned} \quad (12)$$

From (12), the rocking-curve width measured with a parallel pencil beam is approximately

$$\omega \cong [\Delta\theta^2(T_0) + \omega_a^2]^{1/2}, \quad (13)$$

where T_0 is the thickness of the crystal and ω_a is the Darwin width of the reflection used.

3. Interpretation of the model

For symmetrical Laue reflections, the asymmetry angle is 0, and (12) reduces to

$$\Delta\theta(T) = \pm(T/R_s)S'_{63}. \quad (14)$$

In this case, if the sagittal bending axis is perpendicular to a mirror plane, $S'_{63} = 0$, then the expansion of the rocking-curve width due to bending is zero. The crystal's rocking-curve width is then close to the Darwin width of the reflection. This is desirable if high energy resolution is needed, although, as demonstrated earlier, symmetrical Laue crystals do not focus X-rays sagittally.

How various effects contribute to the overall rocking-curve width is expressed through (8), (11), and (12). The second term in (12) [same as in (11)], owing to the change in lattice d spacing, is approximately a factor of $\tan\theta_B$ smaller than the contributions of the lattice rotation. Typical sagittally bent Laue monochromators for high-energy X-rays utilize large asymmetry angles for the necessary focusing (focal length is inversely proportional to $\sin\chi$), and low-index reflections for optimum reflectivity. The Bragg angle for these reflections typically is a few degrees. Thus, the lattice-tilt term [equation (8)] is the dominant part of the rocking-curve width.

In (8), $(S'_{13} - CS'_{23})\sin\chi\cos\chi$ represents the tilting of the lattice planes through the crystal's depth owing to sagittal bending ($S'_{13}\sin\chi\cos\chi$ term) and anticlastic bending ($CS'_{23}\sin\chi\cos\chi$ term). The term $CS'_{23}\tan(\chi \mp \theta_B)$ can be best understood as the effect of an incident X-ray traveling through the crystal at an angle $\chi \mp \theta_B$ to the crystal's normal, and seeing the lattice plane at different angles, owing to the anticlastic bending in the plane of diffraction. The term $S'_{63}\cos^2\chi$ corresponds to the bowing of the lattice planes in the plane of diffraction, caused by the lack of mirror symmetry across the sagittal-bending plane. Except for the $S'_{13}\sin\chi\cos\chi$ term, which is due to sagittal bending, the other effects also are present in similar forms for meridionally bent Laue crystals (Erola *et al.*, 1990).

Based on this understanding, and ignoring the effect of the d-spacing change at small θ_B, the contribution of the anticlastic bending alone to the rocking-curve width can be estimated as

$$\Delta\theta_m \cong \mp(T_0/R_s)CS'_{23}[\sin\chi\cos\chi + \tan(\chi \mp \theta_B)] \quad (15)$$

and the contribution of the sagittal bending alone is

$$\Delta\theta_s \cong \pm(T_0/R_s)S'_{13}\sin\chi\cos\chi. \quad (16)$$

Although sagittal bending is perpendicular to the diffraction plane, the magnitude of its contribution is comparable to that of anticlastic bending. Most interestingly, the two contributions are of opposite sign. Thus, depending on elastic compliances, the two competing factors could cancel out each other, even at large asymmetry angles, thus raising the possibility for obtaining high energy resolution in sagittal-focusing monochromators.

For example, (12) predicts opposite signs in the $\Delta\theta$ *versus* T coefficients between the 111 reflection in the (100) crystal, and the $3\bar{1}1$ reflection in the (111) crystal (details are discussed later). This is due to the different orientations resulting in S'_{13} and S'_{23} being disparate between the two crystals. The two reflections have similar Bragg angles and asymmetry angles. If they were meridionally bent, the lattice rotations across the depths of the crystals would have the same trend. The predicted sign change between the two crystals struck us as being counterintuitive, warranting careful experimental verification. Thus, we specifically designed a depth-resolved rocking-curve measurement to verify this interesting observation.

4. Depth-resolved rocking-curve measurements

Equation (12) gives the angle by which the crystal needs to rotate to find the Bragg condition for a lamella at a given depth T. The range of angle change from the front to the back surface of the crystal typically is of the order of 10 to 100 μrad, and can be easily determined by a rocking-curve measurement. Such measurements generally provide only the magnitude of $\Delta\theta(T_0)$ in (12) but not the sign. By using low-energy X-rays where absorption is not negligible, thereby causing a measurable difference in intensity between beams diffracted by the front and back of the crystal, sometimes the sign can be determined, especially for reflections with large asymmetry angles (there is no path-length difference for a symmetrical Laue reflection). Sagittally bent crystals are the most relevant ones for high-energy X-ray monochromators. Thus, to reliably verify (12), an experimental method is needed that is applicable for all asymmetry angles at high X-ray energies. This can be achieved by measuring the rocking curves of the crystal with a fine slit in the diffracted beam, to define a small region inside the crystal where the diffraction occurs.

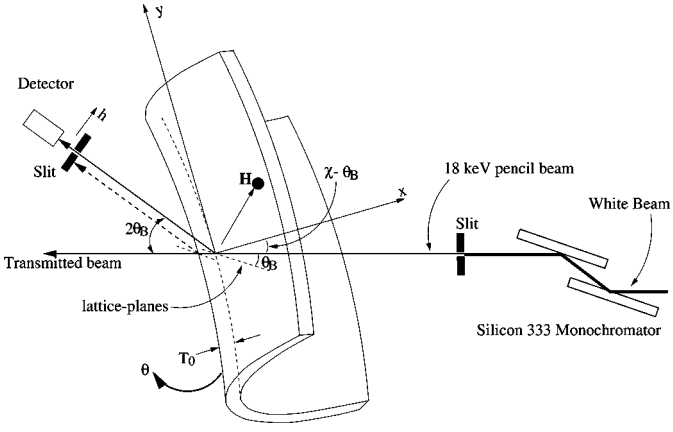

Figure 2
Experimental set-up for measuring the depth-resolved rocking curves.

Experiments were performed at the X15A beamline of the National Synchrotron Light Source (NSLS), Brookhaven National Laboratory, New York. Fig. 2 shows a schematic of the set-up for the depth-resolved rocking-curve measurements. A monochromatic 18 keV X-ray pencil beam, 0.025 mm high and 0.5 mm wide, was prepared using a silicon 333 perfect-crystal monochromator. It was incident in the middle of a sagittally bent Laue crystal. The crystal's tilt angle was adjusted by a two-circle diffractometer. The incident beam's intensity was monitored by an ion chamber while that of the diffracted beam was measured by a scintillation detector on the 2θ arm of the diffractometer. Unlike a conventional rocking-curve set-up, which has a wide-open detector, a horizontal slit, 25 μm in vertical width, was positioned in front of the detector on the 2θ arm, at 100 mm from the crystal.

Conventional rocking curves were then measured with the detector slit removed, by positioning the 2θ arm at the appropriate 2θ value for the reflection being measured, and rotating the crystal around $\chi - \theta_B$ while measuring the intensity of the diffracted X-rays at each angle. Then, with the crystal at the center of the rocking curve, the detector slit was installed and scanned vertically, perpendicular to the diffracted beam, to find the center position where the maximum intensity occurred. Rocking curves, corresponding to the lattice at different depths in the crystal, were subsequently measured with the detector slit at various positions, h, around this center. There is a linear relationship between h and the depth in the crystal, T, where the diffraction occurred. The changes in Bragg angle, $\Delta\theta_B(T)$ [calculated using (11)], due to the change of d spacing across the depth of the crystal typically is smaller by a factor of 10 than the rotation of the lattice planes, and is on the order of a few tens of μrad for the crystals tested. Thus, if the distance between the detector's slit and the crystal is small enough (100 mm in the current case), then the diffracted X-rays can be approximated as being parallel within the depth resolution desired (on the order of 100 μm). With this assumption, for a rocking curve measured with the detector slit at h, the depth, T, of the lattice planes giving rise to that rocking curve is given by

$$T \cong -\frac{h\cos(\chi - \theta_B)}{\sin 2\theta_B}. \qquad (17)$$

In addition to being able to resolve the sign in (12), the measurement of the depth-resolved rocking curve directly determines $\Delta\theta(T)$, independent of the details of X-ray diffraction from each lamella. In contrast to this, the measured rocking-curve width is affected by the Darwin width of the reflection through the dynamical diffraction, and is convoluted with the size/energy/angular distribution of the probe beam. Thus, the calculated value of $\Delta\theta(T_0)$ will approximate the measured width of the rocking curve only if it is much larger than the characteristic width of these effects.

5. Crystals and reflections tested

Perfect silicon crystals, having strong elastic anisotropy and being widely used in monochromators, are the natural choice for testing the model. Depth-resolved rocking curves were measured using different reflections from a sagittally bent silicon (100) crystal (surface perpendicular to the [100] crystallographic direction) and a (111) crystal (surface perpendicular to the [111] direction), so comparisons can be made with the predictions of the model. The orientations of the crystals with respect to the sagittal bending are shown in Figs. 3(*a*) and 3(*b*), for the (100) and (111) crystals, respectively.

The (100) crystal, 0.67 mm thick, was cut from an 8 in-diameter silicon wafer into a square 40 mm high by 100 mm wide, with the short and long sides parallel to the [011] and [$0\bar{1}1$] directions, respectively. Its center active area of 40 mm high by 57 mm wide was bent to a sagittal radius of 760 mm, using a four-bar bender. We previously described the method used for obtaining and verifying a uniform bending, especially around the center of the crystal (Zhong *et al.*, 2001*b*). The sagittal bending axis was along the [011] direction. The resulting meridional bending radius was 18.8 m, determined by measuring the shift in centroid of rocking curves at different positions on the crystal.

Fig. 3(*a*) also shows the accessible low-index reflections in the [$0\bar{1}1$] zone of this crystal. The 333, 111, 133 (χ is positive for these reflections) and their symmetry-related reflections (with χ being negative), such as $\bar{3}33$, were measured in this crystal. The symmetrical 022 reflection was also measured.

The size and thickness of the (111) crystal was the same as the (001) crystal. It was cut from a 6 in silicon wafer with its short and long edges parallel to the [$1\bar{1}0$] and [$11\bar{2}$] directions, respectively. This crystal was sagittally bent along the [$1\bar{1}0$] direction, to a sagittal radius of 760 mm, corresponding approximately to an anticlastic bending radius of 3.9 m. The difference in the anticlastic bending radii between the two crystals is due to the difference in the orientations of the crystals, resulting in drastically different Poisson ratios. Fig. 3(*b*) shows the accessible [$11\bar{2}$] zone reflections, of which the $3\bar{1}1$, $5\bar{3}1$ and $1\bar{3}\bar{1}$ reflections were measured.

For each reflection, rocking curves were measured with the detector slit at 41 different positions covering a range of approximately 1 mm. The vertical height of the diffracted beam, $T_0 \sin 2\theta_B / \cos(\chi - \theta_B)$, was about 0.1 to 0.4 mm, depending on the reflection. When the slit was in a position outside the range of the diffracted beam, the detector recorded no signal at all crystal angles, since the diffracted beam did not reach the detector, even though the crystal might be diffracting at certain tilt angles.

6. Experimental results

As an example, Fig. 4 shows the rocking curves of the 111 reflection in the (100) crystal, measured with the detector slit at positions from −0.125 to 0 mm with a 0.025 mm spacing in between, corresponding to a probed depth, T, of 0.5 to 0 mm, every 0.1 mm. Also shown in Fig. 4 is the rocking curve of the same crystal, taken with the detector slit removed. The rocking curve is roughly rectangular, typical of bent Laue crystals diffracting at high X-ray energies. The rounded edges of the rocking curves are mostly due to the vertical divergence (about 5 μrad) of the incident beam, as a result of a non-zero incident slit height and the vertical size of the synchrotron X-ray source. The rocking curves have a depth sensitivity smaller than 10 μm. The peak reflectivity of each depth-resolved rocking curve corresponds approximately to the reflectivity of the rocking curve by the whole crystal. This, and the progression of the rocking-curve position with the probed depth, suggest that the behavior of the bent crystal is consistent with lamellar model, with its lattice planes at different depths diffracting at different tilt angles.

For each depth-resolved rocking curve, the depth in the crystal where the diffraction occurred was calculated using (17). The centroid of the curve was calculated using the average of the FWHM positions on the curve. The centroids

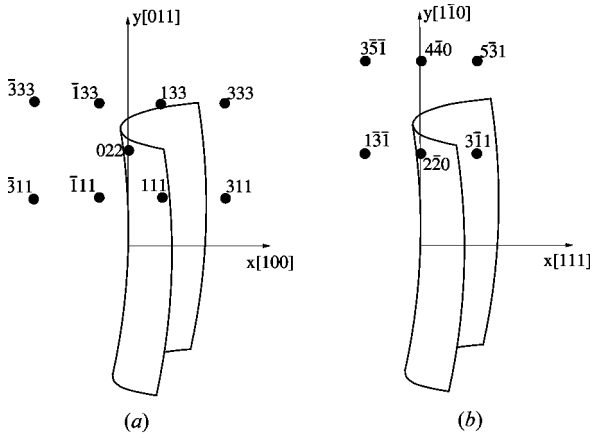

Figure 3
Real- and reciprocal-space configurations for two crystals of different orientations used for depth-resolved rocking-curve measurements. (*a*) A (100) crystal, sagittally bent along the [011] direction, and diffracting in the [$0\bar{1}1$] zone. (*b*) A (111) crystal bent along the [$1\bar{1}0$] direction and diffracting in the [$1\bar{1}2$] zone.

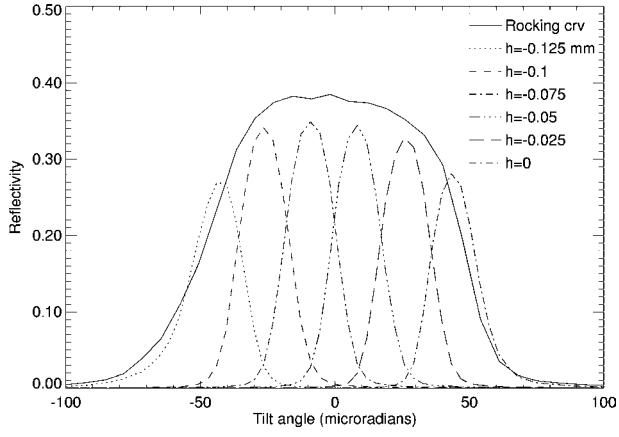

Figure 4
Depth-resolved measurements on the 111 reflection in the (100) crystal. The broken lines show rocking curves measured with the detector slit at various positions. The solid line shows the rocking curve taken after removing the slit in front of the detector.

Table 1
Parameters used, and results obtained, for different reflections on (100) and (111) crystals.

Crystal	(100)							(111)		
S'_{13}	−0.36							−0.16		
S'_{23}	−0.061							−0.26		
S'_{63}	0							0		
CS'_{23}, meas.	−0.040							−0.19		
Reflection	111	$\bar{1}11$	333	$\bar{3}33$	133	$\bar{1}33$	022	$3\bar{1}1$	$1\bar{3}\bar{1}$	$5\bar{3}1$
χ (°)	35.3	−35.3	35.3	−35.3	13.3	−13.3	0	31.5	−31.5	17.0
θ_B (°)	6.3	6.3	19.2	19.2	16.0	16.0	10.3	12.1	12.1	22.0
$\Delta\theta_B(T_0)$ (μrad)	14	14	45	45	14	14	6.4	35	35	69
$\Delta\theta_{rot}(T_0)$ (μrad)	114	−102	124	−84	65	−44	6.4	−73	177	6.8
$\Delta\theta(T_0)$ (μrad)	−100	117	−78	130	−51	58	0	109	−142	62
ω, theo. (μrad)	101	118	78	130	51	62	10	109	142	62
FWHM, meas. (μrad)	96	119	76	124	55	63	23	112	138	72
$\Delta\theta/T$, theo. (μrad mm^{-1})	−149	174	−116	194	−76	87	0	163	−212	93
$\Delta\theta/T$, meas. (μrad mm^{-1})	−175	177	−137	186	−95	80	−19	169	−244	76

then were subtracted by the centroid of the rocking curve corresponding to $T = 0$, for the measured reflections on the (100) and (111) crystals, respectively. Since the smaller Bragg angles of the low-index reflections lead to a larger change of depth for the same step in the detector slit, there are less data points for the low-index reflections than for the high-index ones. As seen in Figs. 5 and 6, for each reflection, the relationship between the rocking-curve position and the depth in the crystal is approximately linear, as predicted by (12). The slope of the curves, both in magnitude and sign, are sensitive to the asymmetry angle and the orientation of the crystal.

The theoretical relationship between the rocking-curve centroid and the depth can be derived using (12). Since the sagittal bending is on the positive side of the x axis, the sagittal radius, R_s, is positive for both crystals. All reflections measured correspond to the upper-sign case, with χ being positive for the reflections in the first quadrant and negative for reflections in the second quadrant.

The parameters of elastic compliances for the bent crystals were obtained by a transformation of the stress–strain tensor of the principal compliances for silicon (Wortman & Evans, 1965). The S'_{63} is zero for both crystals owing to the high symmetry of the crystal's orientation. Values for CS'_{23} were obtained using $CS'_{23} = R_s/R_m$; they are −0.040 and −0.19, respectively, for the (100) and (111) crystals. The factor C, which summarizes the effects of the boundary conditions on the crystal, is typically 0.2–1 depending on the crystal shape and the bending mechanism. With the theoretical S'_{23} and the measured CS'_{23}, the C values are 0.66 and 0.72 for the (100) and (111) crystals, respectively. Similar C values were observed for the two crystals because they have the same size and thickness, and were bent with similar benders.

Using these parameters, the rocking-curve positions as a function of depth in the crystal were calculated for all the reflections, using (12). The results are plotted as lines in Fig. 5 for reflections in the (100) crystal, and in Fig. 6 for reflections in the (111) crystal. The trends and absolute magnitude of the experimental values agree with the theoretical ones within about 20 μrad.

Table 1 gives details of the parameters used and the results for all measured reflections. $\Delta\theta(T_0)$ across the crystal thickness of 0.67 mm was calculated using (12). The contribution of

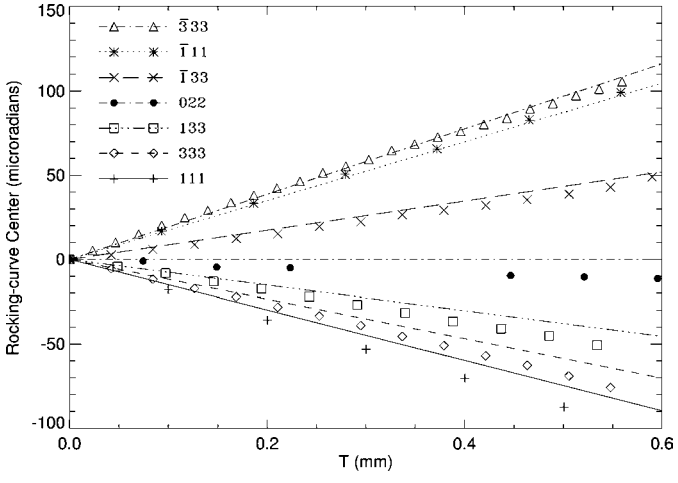

Figure 5
Centroids of the depth-resolved rocking curves *versus* the depths in the crystal where they were measured. Results are shown of the 333, 111, 133, $\bar{3}33$, $\bar{1}11$, $\bar{1}33$ and 022 reflections on the (100) crystal. The lines show the theoretical results.

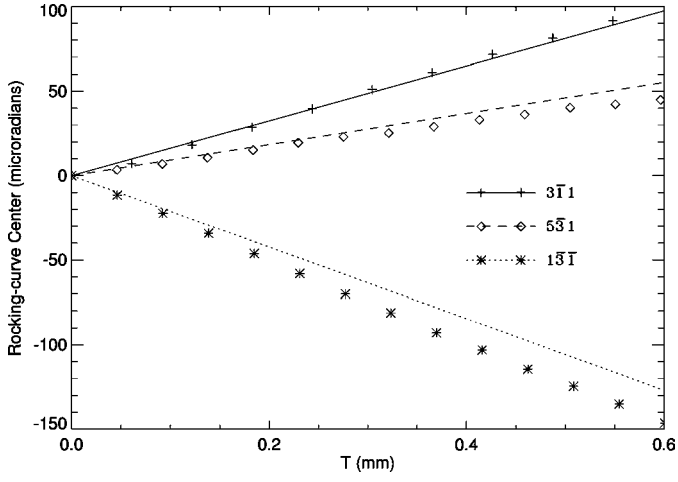

Figure 6
Results obtained for the $3\bar{1}1$, $1\bar{3}\bar{1}$ and $5\bar{3}1$ reflections on the (111) crystal, showing the centroids of the depth-resolved rocking curves *versus* the depth in the crystal. The lines show the theoretical relationship.

d-spacing change [$\Delta\theta_B$, calculated using (11)] and rotation of the lattice planes [$\Delta\theta_{\rm rot}$, calculated using (8)] are shown, so their relative magnitudes can be compared. The rocking-curve widths, ω, calculated using (13), are compared with the FWHM of the measured rocking curves. Agreement between them, except for the 220 reflection, is within 5 μrad.

The measured $\Delta\theta/T$ values were obtained by a linear least-squares fit to the experimental data shown in Figs. 5 and 6. The signs of the theoretical $\Delta\theta/T$ agree with the measured ones, and the absolute values agree within 20%. The discrepancies are probably due to the assumption in (17) that the diffracted X-rays are exactly parallel. Also, the small coefficient, $\tan 2\theta_B$, in (17) magnifies errors in h when calculating T. Despite these known errors, the overall agreement between the model and experiment is satisfactory, considering that no free parameters were used for the theoretical calculations.

Comparing the solid lines and the associated experimental points in Figs. 5 and 6 shows that there is, indeed, a change of sign in the $\Delta\theta$ *versus* T relationship between the 111 reflection in the (100) crystal and the $3\bar{1}1$ reflection in the (111) crystal. This finding further demonstrates the uniqueness of sagittally bent Laue crystals and the necessity of considering elastic anisotropy for this class of crystals.

7. Concluding remarks

We have shown that sagittal bending typically broadens the angular width of the X-ray diffraction by a Laue crystal. The crystal's lattice orientation, anisotropic elastic properties and asymmetry angle all play important roles in determining the extent of this broadening. We developed an analytical model for sagittally bent Laue crystals to explain the broad range of X-ray rocking-curve widths measured using different reflections from crystals of different orientations. The model allows insight into the complex coupling between sagittal and meridional bending, the role of anisotropy, and their effects on crystal diffraction. Silicon crystals of two representative high-symmetry orientations were tested using a method of depth-resolved rocking-curve measurement, specifically designed to verify the model. The model reliably predicted the extent of broadening of the measured rocking curves.

The discussion of the experimental results illustrates the rich set of diffraction properties attainable by bent Laue crystals. The measured variation from the front to the back of each crystal covers a wide range between −150 and 150 μrad, suggesting the possibility of fine-tuning the diffraction properties by varying the asymmetry angle and crystal orientation. The model allows these properties to be tailored by properly designing the monochromator, most notably through crystal orientation, to suit different experimental needs, which often vary in the requirements on flux (related to integrated reflectivity) and resolution (related to anticlastic bending radius and rocking-curve width).

We have only measured the combined effects of lattice rotation and d-spacing change. By utilizing an analyzer crystal after the detector slit, the lattice rotation and d-spacing change effects can be separated.

Although the discussions have been carried out with reference to X-ray diffraction, and the experimental verification of the model was done using X-rays, the model should apply equally well to neutrons with little modification.

The depth-resolved rocking-curve measurements show that one of the basic assumptions of the lamellar model, *i.e.* the gradual change of the Bragg condition across the depth of the crystal, is still valid for sagittally bent Laue crystals. Thus the broadening of the rocking curve [equation (12)] obtained from the model can be incorporated into the lamellar model to predict the reflectivity of a sagittally bent crystal.

This work was supported by funding from the US Department of Energy, DE-AC02-76CH00016. The authors would like to thank Lonny Berman, Grant Bunker, Wolfgang Caliebe, Dean Chapman, Dean Haeffner, Erik Johnson, Ulrich Lienert and William Thomlinson for helpful discussions about the work, and Avril Woodhead for critical comments on the manuscript.

References

Albertini, G., Boeuf, A., Cesini, G., Mazkedian, S., Melone, S. & Rustichelli, F. (1976). *Acta Cryst.* A**32**, 863.
Boeuf, A., Lagomarsino, S., Mazkedian, S., Melone, S., Puliti, P. & Rustichelli, F. (1978). *J. Appl. Cryst.* **11**, 442–449.
Caciuffo, R., Melone, S., Rustichelli, F. & Boeuf, A. (1987). *Phys. Rep.* **152**, 1–71.
Chukhovskii, F. N., Chang, W. Z. & Förster, E. (1994). *J. Appl. Cryst.* **27**, 971–979.
Egert, V. G. & Dachs, H. (1970). *J. Appl. Cryst.* **3**, 214–220.
Erola, E., Eteläniemi, V., Suortti, P., Pattison, P. & Thomlinson, W. (1990). *J. Appl. Cryst.* **23**, 35–42.
Hartlaub, S. (1996). Diplomarbeit dissertation, Fachhochschule Heilbronn, Germany.
Hiraoka, N., Itou, M., Ohata, T., Mizumaki, M., Sakurai, Y. & Sakai, N. (2001). *J. Synchrotron Rad.* **8**, 26–32.
Kalman, Z. H. & Weissmann, Z. (1983). *J. Appl. Cryst.* **16**, 295–303.
Krisch, M., Freund, A., Marot, G. & Zhang, L. (1991). *Nucl. Instrum. Methods Phys. Res. A*, **305**, 208–213.
Lienert, U., Schulze, C., Honkimaki, V., Tschentscher, T., Garbe, S., Hignette, O., Horsewell, A., Lingham, M., Poulsen, H., Thomsen, N. B. & Ziegler, E. (1998). *J. Synchrotron Rad.* **5**, 226–231.
Mikula, P., Kulda, J., Vrana, M. & Chalupa, B. (1984). *J. Appl. Cryst.* **17**, 189–195.
Popovici, M., Stoica, A. D., Chalupa, B. & Mikula, P. (1988). *J. Appl. Cryst.* **21**, 258–265.
Quintana, J. P., Kushnir, V. I. & Rosenbaum, G. (1995). *Nucl. Instrum. Methods Phys. Res. A*, **362**, 592–594.
Schulze, C., Lienert, U., Hanfland, M., Lorenzen, M. & Zontone, F. (1998). *J. Synchrotron Rad.* **5**, 77–81.
Suortti, P. & Schulze, C. (1995). *J. Synchrotron Rad.* **2**, 6–12.
Voigt, W. (1928). *Lehrbuch der Kristallphysik*, equation 178. Leipzig: B. G. Teubner.
Wortman, J. J. & Evans, R. A. (1965). *J. Appl. Phys.* **36**, 153–156.
Yoneda, Y., Matsumoto, N., Furukawa, Y. & Ishikawa, T. (2001). *J. Synchrotron Rad.* **8**, 18–21.
Zhong, Z., Kao, C. C., Siddons, D. P. & Hastings, J. B. (2001*a*). *J. Appl. Cryst.* **34**, 504–509.
Zhong, Z., Kao, C. C., Siddons, D. P. & Hastings, J. B. (2001*b*) *J. Appl. Cryst.* **34**, 646–653.